Earth Surf. Dynam. Discuss., 3, 1–52, 2015
www.earth-surf-dynam-discuss.net/3/1/2015/
doi:10.5194/esurfd-3-1-2015

Earth Surface Dynamics Discussions
Open Access

Spatial distributions of earthquake-induced landslides and hillslope preconditioning in northwest South Island, New Zealand

R. N. Parker[1], G. T. Hancox[2], D. N. Petley[3], C. I. Massey[2], A. L. Densmore[4], and N. J. Rosser[4]

[1]School of Earth and Ocean Sciences, Cardiff University, Cardiff, UK
[2]Institute of Geological and Nuclear Sciences (GNS), Lower Hutt, New Zealand
[3]School of Environmental Sciences, University of East Anglia, Norwich, UK
[4]Institute of Hazard, Risk and Resilience, Durham University, Durham, UK

Received: 17 November 2014 – Accepted: 26 November 2014 – Published: 6 January 2015

Correspondence to: R. N. Parker (parkerr5@cardiff.ac.uk)

Published by Copernicus Publications on behalf of the European Geosciences Union.

Abstract

Current models to explain regional-scale landslide events are not able to account for the possible effects of the legacy of previous earthquakes, which have triggered landslides in the past and are known to drive damage accumulation in brittle hillslope materials. This paper tests the hypothesis that spatial distributions of earthquake-induced landslides are determined by both the conditions at the time of the triggering earthquake (time-independent factors), and also the legacy of past events (time-dependent factors). To explore this, we undertake an analysis of failures triggered by the 1929 Buller and 1968 Inangahua earthquakes, in the northwest South Island of New Zealand. The spatial extent of landslides triggered by these events was in part coincident (overlapping). Spatial distributions of earthquake-triggered landslides are determined by a combination of earthquake and local characteristics, which influence the dynamic response of hillslopes. To identify the influence of a legacy from past events, we use logistic regression to control for the effects of time-independent variables (seismic ground motion, hillslope gradient, lithology, and the effects of topographic amplification caused by ridge- and slope-scale topography), in an attempt to reveal unexplained variability in the landslide distribution. We then assess whether this variability can be attributed to the legacy of past events. Our results suggest that the 1929 Buller earthquake influenced the distribution of landslides triggered by the 1968 Inangahua earthquake. Hillslopes in regions that experienced strong ground motions in 1929 were more likely to fail in 1968 than would be expected on the basis of time-independent factors alone. This effect is consistent with our hypothesis that unfailed hillslopes in the 1929 earthquake were weakened by damage accumulated during this earthquake and its associated aftershock sequence, and this weakening then influenced the performance of the landscape in the 1968 earthquake. While our results are tentative, the findings emphasize that a lack of knowledge of the damage state of hillslopes in a landscape potentially represents an important source of uncertainty when assessing landslide susceptibility.

ESURFD

3, 1–52, 2015

Constraining the damage history of hillslope materials, through analysis of historical events, therefore provides a potential means of reducing this uncertainty.

1 Introduction

Regional landslide-hazard assessments rely on models that upscale our conceptual understanding of fundamental controls on landslides, through analysis of the influence of different proxy variables on landslide occurrence (e.g., Capolongo et al., 2002; Garcia-Rodriguez et al., 2008). Most studies to date have addressed spatial correlations between the distribution of landslides and variables that provide proxies for seismic ground motions and the modelled stability of hillslopes (e.g.: Dai et al., 2011; Meunier et al., 2008, 2007). These studies implicitly rely upon a static model of hillslope sensitivity to landslide triggering. In other words, the predicted number of landslides triggered by any given trigger event will not vary through time. However, this assumption is at odds with observations of increased rainfall-triggered landslide activity above baseline rates observed in the wake of large earthquakes (Hovius et al., 2011; Saba et al., 2010; Tang et al., 2011). Similarly, data from the 2010–2011 Canterbury earthquake sequence reveal landslide triggering at lower ground accelerations following the February 2011 earthquake, which caused cracks to develop in hillslopes that subsequently failed in later earthquakes in the sequence (Massey et al., 2014a, b). These observations suggest that hillslopes may retain damage from past earthquakes, which makes them more susceptible to failure in future triggering events. Note that here we define failure as the total collapse of a hillslope where the failed mass evacuates the failure plane and moves downslope to leave a discernable, bare-earth scar. According to the classification of Keefer (1984, 2002), these types of failures are generally grouped as disrupted slides, given the significant internal disruption exhibited by the landslide mass. From the classification system of Varnes (1978) (updated by Hungr et al., 2014), this group includes rock and debris falls and slides, and rock avalanches.

ESURFD
3, 1–52, 2015

Globally disrupted landslides are estimated to comprise the majority, ∼ 86 %, of reported earthquake-induced landslides (Keefer, 1984, 2002).

One mechanism by which hillslopes could be made more susceptible to failure is progressive brittle damage accumulation in hillslope materials, whereby permanent slope displacement leads to cracking and dilation of the mass. Damage accumulation occurs near the surface within hillsopes (Clarke and Burbank, 2011), as gravitational stress coupled with seismically- and hydrologically-induced changes in the stress distribution drive strain-dependent weakening via a progressive mechanism of failure (Petley et al., 2005; Leroueil et al., 2012). Brittle deformation of this type has been observed in soil at low confining pressures (1–250 kPa), in mudrocks at confining pressures up to 2 MPa, and at greater confining pressures in harder geological materials (Petley and Allison, 1997; Evans et al., 2013). As this mechanism occurs in the fabric of brittle rock or cohesive soils (bonded or cemented materials, where strain is localized during failure) it is likely to be common to most disrupted types of landslide induced by earthquakes. Exceptions to this are shallow colluvial failures in cohesionless soil (Selby, 2005) and cases of failure in very poor quality, soft rock masses or soft layers (Hoek et al., 2002), where material behaves in a ductile manner (Petley and Allison, 1997). Where earthquake-induced landslide failure develops progressively, via brittle deformation, hillslopes may retain damage from past earthquakes. Whether or not a hillslope fails in response to an earthquake will be a function of both the current event, and by definition, the history of damage accumulated in that hillslope from previous events. The absence of this historical information from landslide analyses and predictive models potentially represents a significant gap in our understanding of factors that control the distribution of landsliding.

If previous earthquakes do influence patterns of landsliding in subsequent earthquakes, then it is reasonable to hypothesize that spatial distributions of landslides should be at least partially correlated with the ground motions from past earthquakes. In order to investigate the role of hillslope damage history in conditioning landslide distributions, we test this hypothesis through analysis of the spatial distribution of land-

ESURFD
3, 1–52, 2015

slides triggered by two large ($M_w > 7$) earthquakes, which occurred in close proximity in the northwest South Island of New Zealand. First, we present inventories of landslides triggered by the 1929 Buller and 1968 Inangahua earthquakes. Second, we undertake a spatial analysis of the distributions of both events, using logistic regression. Third, we use the results of this analysis to test the influence of the 1929 earthquake on the distribution of landslides triggered by the 1968 earthquake.

2 The 1929 Buller and 1968 Inangahua earthquakes

The 17 June 1929 Buller (Murchison) earthquake ($M_w = 7.7$; Dowrick and Rhoades, 1998; Dowrick, 1994) and the 24 May 1968 Inangahua earthquake ($M_w = 7.1$; Anderson et al., 1994), both triggered landslides over a large area (Fig. 1). The epicentres of the two earthquakes were ∼ 21 km apart, whilst at their closest point the mapped surface expressions of the coseismic faults lie 7 km apart. The earthquakes have very similar reverse thrust focal mechanisms, with small components of left-lateral strike-slip. Isoseismal maps (Dowrick, 1994; Adams et al., 1968) suggest that ground motions from the two events had a MMI VIII overlap area of ∼ 3505 km^2 and a MMI IX overlap area of ∼ 584 km^2 (Fig. 1).

2.1 Coseismic sources and ground motion

The White Creek fault has been identified as the source of the 1929 earthquake, although surface faulting was only observed along an 8 km length of the fault (Fyfe, 1929; Henderson, 1937). Back analysis of seismic data (Doser et al., 1999), ground motion intensities (Dowrick, 1994), and coseismic landslides (Pearce and O'Loughin, 1985; Hancox et al., 2002) suggest a unilateral rupture extending 30–50 km to the north of the epicentre. This corresponds with the mapped geological (ground surface) trace of the White Creek fault. Estimates of dip angle range from 60–70° based on surface displacement observations (Henderson, 1937), to 46 ± 13° based on inversion of data from

ESURFD
3, 1–52, 2015

seismic stations (Doser et al., 1999), and 45° based on elastic dislocation modelling (Haines, 1991). Doser et al. (1999) inferred a focal depth of 9 ± 3 km. To approximate the 1929 seismic source geometry in our analysis, we use the surface fault line and fault parameters of the White Creek fault as used in the New Zealand probabilistic seismic hazard model (Stirling et al., 2007, 2000, 2002, 2012; Berryman, 1980; Haines, 1991). This model assumes a fault plane striking 015°, and dipping at 45° from the surface to a maximum depth of 12 km, with a dip direction of 100°.

The seismic source geometry of the 1968 earthquake has been constrained through an integrated geological, geodetic and seismological source model (Anderson et al., 1993, 1994). We use a single fault plane trending northeast (25°), dipping at ∼ 45° from a depth of 10–15 km to within ∼ 1 km of the surface (i.e. no primary ground surface rupture), with a dip direction of 295° extending around 30 km in length (Anderson et al., 1993, 1994).

As coseismic landslide occurrence is driven by seismic shaking, it is important that we constrain the spatial pattern of ground accelerations. The strength of seismic ground accelerations attenuates with distance from the seismic source (Abrahamson et al., 2008; Campbell and Bozorgnia, 2008). However, the regional distribution of ground acceleration is also subject to the effect of rupture directivity and regional variation in the damping effect of earth materials (ibid.). In an attempt to account for these effects in the case of the 1968 earthquake, we also make use of the USGS Shakemap output for this event (USGS, 2014). This Shakemap is based on the fault model described above, and uses ground motion data from 15 seismic stations across New Zealand (three of which are within or just beyond the area of landslide mapping conducted here, Fig. 1), as well as estimates of PGA derived from reports at 159 additional sites. Although this model is still subject to uncertainty, by incorporating observed ground motions and site amplification factors, it can potentially provide a more accurate representation of the regional distribution of ground motion. PGA estimates derived from scratch-plate records at Reefton, Westport and Murchison report ground

ESURFD
3, 1–52, 2015

accelerations of 0.58, 0.30 and 0.36 g respectively (Adams et al., 1968; Dowrick and Sritharan, 1993), with which the Shakemap dataset is consistent.

3 Earthquake-induced landslides

Both earthquakes triggered widespread landsliding throughout the area that experienced intensities of MMI = VIII to X. We review the types of landslides triggered by the earthquakes and outline our methodology for producing landslide inventories for the two events.

3.1 Landslide types

Most failures triggered by these earthquakes were disrupted rock and debris slides, rockfalls and rock avalanches, with very few coherent landslides and lateral spreads seen in the field or in aerial photos (Hancox et al., 2014, 2002). In Figs. 2–6 we present examples of these different landslide types from the two earthquakes. Note that an extended review of major landslides and landslide types is presented in Hancox et al. (2014).

Rockfalls were commonly triggered on steep scarps of tertiary limestone, granite and greywacke, with numerous failures ranging from individual, small boulders to large falls of 10^5 m^3 (Fig. 2). Debris slides were the most frequent type of landslide triggered by the earthquakes and were common in areas of granite and greywacke (Fig. 3). Several examples of large rock avalanches were triggered by the earthquakes. The 1929 earthquake triggered the 18 million m^3 Lake Stanley rock avalanche (Fig. 4a), in Palaeozoic conglomerate and volcanics around 90 km north of the epicentre. Although this landslide is 35 km north of the present study area and is not included in the 1929 landslide dataset (which covers only the southern half of the landslide-affected area) it is typical of the ten largest landslides that occurred in 1929 (Hancox et al., 2002). The landslide is around ~ 2 km long with an elevation range of 800 m. The largest landslide

ESURFD
3, 1–52, 2015

triggered by the 1968 earthquake was a 5 million m^3 rock avalanche (Fig. 4b). This failure occurred in weathered granite, running out about 1.2 km to the valley floor and about 100 m up the opposite side of the valley.

Several large rockslides were also triggered by the earthquakes. For example, the 1929 earthquake triggered the 18 million m^3 Matakitaki landslide (Hancox et al., 2002). This dipslope rockslide travelled ~ 1 km across the valley floor, destroying two farm houses and killing 4 people, and formed a landslide dam (Fig. 5a). Figure 5b shows the intensity of landslide damage in the Matiri Valley, an area close to the seismogenic fault, where landslide scars from 1929 are still clearly visible today. The 1968 earthquake triggered the 3 million m^3 Oweka rockslide; a disrupted mass of muddy sand stones that fell from a vegetation-covered slope (Fig. 6a). The largest (2.8 million m^3) rotational landslide triggered by the 1968 earthquake occurred on a 100 m high terrace in sandy ("Blue Bottom") mudstone (Fig. 6b).

In most of these failure types, we might reasonably expect the process of material failure to involve some component of brittle deformation, given the low temperature and confining pressure in near-surface materials. Notable exceptions to this may include structurally-controlled failures along ductile bedding planes. For example, field observations from the Oweka landslide suggest that, for a large semi-intact section of the landslide, the mechanism of movement was sliding on an extensive bedding plane coated with a thin layer of plastic clay. Among debris (colluvium) failures, the failure mode will vary, depending on the material content and whether failure took place in brittle or ductile zones.

3.2 Production of landslide inventories

In order to produce regional inventories of landslides triggered by these events, landslide scars were identified and mapped through stereoscopic interpretation of panchromatic aerial photographs, combined with ground and oblique aerial photography, based on morphometric criteria and the surface reflectivity contrasts between undisturbed

ESURFD
3, 1–52, 2015

ground and failures (Nichol and Wong, 2005; Liu et al., 2002; Hovius et al., 1997). Our inventories consist of landslides where the failed mass evacuated the failure plane and moved downslope to leave a discernable, bare-earth scar. Accordingly, all landslides included in the inventories are disrupted slides, which moved rapidly downslope following failure.

Landslides triggered by the 1929 earthquake were mapped using 1 : 86 000 scale images taken in February 1968, and validated using ground photos taken in 1929 and further aerial photos taken in 1947 (SN 265, Runs 1457–1463) for selected regions (Appendix A). From comparison of earlier and later imagery, we found that scars from landslides triggered in 1929 were still clearly visible and could be mapped in imagery acquired 39 years after the earthquake, due to a slow rate of regeneration of native bush. This is particularly true for larger, bedrock failures, while smaller soil and debris failures are more rapidly obscured by vegetation. Landslides attributed to the 1968 earthquake were mapped using 1 : 66 660 scale panchromatic aerial images (Appendix A) taken in November 1974 and aerial oblique and ground photos taken in 1968–1969. Landslide mapping was further validated based on observations from fieldwork undertaken by G. Hancox throughout 1968 and 1969, and during aerial reconnaissance undertaken by G. Hancox in 1998 and 2010, and in 2011 by R. Parker.

Comparison of pre- and post-1968 imagery was carried out to delineate 1929 landslide areas from those triggered or further influenced by the 1968 earthquake (Fig. 7). Although the intervening periods between seismic events and imagery acquisition create potential for inclusion of landslides triggered by aseismic (rainfall) events, observations from reconnaissance between 1968 and 2014 and historical records compiled by the West Coast Regional Council (Hancox et al., 2014) suggest a lack of widespread landsliding resulting from heavy rainstorms or other processes during inter-seismic periods, supporting a seismic mode of triggering for the landslides observed (Pearce and O'Loughin, 1985; Hancox et al., 2014). Prior to the 1929 earthquake, two large events of $M_w \sim 7$ are estimated to have occurred in 1868 and 1893, with epicentres located around 200 km to the north and north-east of the study area, respectively (Anderson

ESURFD
3, 1–52, 2015

et al., 1994). Due to the lack of pre-1929 imagery, there may be potential for landslides triggered by these events to be wrongly attributed to the 1929 earthquake. However, due their distance from the study area, these events would have produced relatively weaker ground motions than the 1929 event – MMI V to VII (1868,1893) vs. MMI IX to X (1929) (Anderson et al., 1994; Hancox et al., 2002) – capable of triggering few, relatively small landslides (Hancox et al., 2002). As small landslides are rapidly obscured by vegetation, it is unlikely that smaller failures from these events feature in our dataset. An earlier larger earthquake of around $M = 7.4$ is also thought to have occurred c.1650, as indicated by several landslide-dammed lakes in the northwest Nelson area (Hancox et al., 2002; Perrin and Hancox, 1992; Henderson, 1937). Larger, visible pre-20th century landslide scars in the region were mapped separately and are not included in this analysis.

Polygons delineating the combined landslide source and runout areas of individual landslides were mapped by hand on 1 : 50 000 scale topographic maps, which were then digitized and imported into a GIS. Particular effort was made to map individual failures separately and separate coalesced landslide features, in order to avoid issues of feature amalgamation in the dataset (Li et al., 2014). The imagery resolution allowed mapping of landslides down to a minimum size of $\sim 50\,\text{m} \times 50\,\text{m}$ ($\sim 2500\,\text{m}^2$). For the 1929 earthquake, 4074 landslides ($182\,\text{km}^2$ total landslide area) were mapped across an area of $4222\,\text{km}^2$. Note that this mapping covers the southern half of the landslide affected area, while the 1929 landslides extend to the north, away from the region affected by the 1968 earthquake. By contrast, for the 1968 Inangahua earthquake only 1400 landslides ($39\,\text{km}^2$ total landslide area) were mapped across an area of $\sim 3500\,\text{km}^2$. Of these, 246 landslides were reactivations or enlargements of landslide scars that failed in 1929, mostly in over-steepened source areas of the pre-existing failures. The areal extents of the landslide inventories overlap by $2882\,\text{km}^2$, $\sim 80\,\%$ of which experienced MMI $\geq$ VIII in both events. The areas of both the 1929 and 1968 landslides exhibit characteristic power-law scaling (e.g. Hovius et al., 1997; Guzzetti

ESURFD
3, 1–52, 2015

et al., 2002; Malamud et al., 2004; Van Den Eeckhaut et al., 2007) (Fig. 8):

$$p(x) = \frac{\alpha - 1}{x_{\min}} \left(\frac{x}{x_{\min}} \right)^{-\alpha} \quad (1)$$

where $x_{\min}$ is the minimum size of landslide modelled by the function and α is the power-law scaling exponent. The positions of the rollover for smaller landslides suggest complete mapping of landslides larger than 11 000 m^2 in both datasets. More rapid vegetation recovery on smaller landslide scars is likely to censor the landslide inventory below this threshold. The power-law scaling exponents of 2.68 (1929) and 2.85 (1968), fitted using the method of Clauset et al. (2009), fall within the typical range of previously-observed values for landslide inventories (1.4 to 3.4), which have a central tendency around 2.3 to 2.5 (Van Den Eeckhaut et al., 2007; Stark and Guzzetti, 2009). The fact that the scaling exponents are slightly higher than the global mean is likely to be a reflection of efforts to map individual failures separately.

To analyse the spatial pattern of hillslope failures, we use the landslide source areas, rather than areas covered by landslide runout and deposits. For most landslides it was difficult to visually separate landslide source and runout or deposit area. Based on a sample of 51 landslides where visual delineation of the source area was possible, dividing the extent of each landslide at its midpoint elevation (i.e.: the contour halfway been the maximum and minimum landslide elevation) provided a good approximation of the separation between source and runout-deposit (Appendix B). This approach is similar to the method of extracting landslide areas above the median landslide elevation, which has been employed in previous studies (Parise and Jibson, 2000; Jibson et al., 2000; Capolongo et al., 2002; Lee et al., 2012). However, our technique is less prone to overestimation of the source area for landslide masses that runout over large distances across low gradient ground.

ESURFD
3, 1–52, 2015

4 Investigating controls on the spatial distribution of landslides

Distributions of earthquake-induced landslides are dependent on factors that influence the dynamic response of hillslopes undergoing seismic shaking (e.g.: Jibson, 2011; Newmark, 1965). These factors can be broadly grouped into those that influence the intensity of seismic ground motions, the strength of hillslope materials, and the static shear stress. Empirical studies have revealed a number of proxy variables that can be used to represent these factors at the regional scale (Table 2).

Logistic regression is a standard technique for assessing controls on earthquake-triggered landslide distributions (e.g., Yesilnacar and Topal, 2005; Dai and Lee, 2003; Garcia-Rodriguez et al., 2008; von Ruette et al., 2011), by modelling the influence of multiple predictor variables on a categorical response (Cox, 1958; Walker and Duncan, 1967). The function takes the form:

$$P(Y = 1) = \frac{1}{1 + e(-(b_0 + b_1x_1 + b_2x_2 + b_3x_3 \ldots b_nx_n))} \quad (2)$$

where logistic regression is used to estimate the coefficients $(b, b_n \ldots)$ for predicting the probability that $Y = 1$, given the values of one or more predictor variables $(x, x_n \ldots)$. In this case, $Y = 1$ corresponds to the occurrence of a landslide at a particular point in space.

Although previous studies have applied logistic regression with the implicit assumption of temporally static hillslope sensitivity to landslide triggering, here we use this technique to test a hypothesis of hillslope preconditioning for failure by previous events. We first undertake an implicitly static logistic regression analysis in order to model the distributions of landslides, as can best be achieved without considering the influence of past events. We hypothesize that if the 1929 earthquake influences the 1968 landslide distribution, then the residual variability, unexplained by our regression model, must exhibit a relationship with the spatial distribution of the effect of the previous earthquake on hillslopes. To test this hypothesis, we compare the residuals of our 1968 regression with a measure of hillslope preconditioning, here the probability of landslide occurrence

ESURFD
3, 1–52, 2015

in 1929. A graphical representation of hypothetical outcomes is presented in Fig. 9. We assume that logistic regression models have been fitted and used to hindcast the probability of hillslope failure (P_{ls}) for both earthquakes. If the model for the 1968 earthquake is accurate, then the residuals (observed P_{ls} minus predicted P_{ls}) should yield no structure when plotted against the predicted values (Fig. 9a). Similarly, there should be no structure in the residuals when plotted against each of the individual predictor variables (Fig. 9b). However, if the 1929 earthquake has influenced the 1968 landslide distribution, then the residuals should exhibit structure when plotted against the predicted P_{ls} for the 1929 earthquake. Figure 9c illustrates two end-member scenarios, showing how the 1929 earthquake might be expected to influence the 1968 landslide distribution:

1. *Hillslopes with higher predicted P_{ls} in 1929 exhibit lower than expected P_{ls} in 1968.* This could be the case if widespread failure of unstable hillslopes in 1929 resulted in fewer hillslopes being "available" for failure in 1968, or;

2. *Hillslopes with higher predicted P_{ls} in 1929 exhibit higher than expected P_{ls} in 1968.*
   This could be the case if, despite the widespread failure of unstable hillslopes in 1929, damage accumulation in those hillslopes that did not fail effectively primed those sites for later failure in 1968.

Conversely, if there were no structure in the residuals, this would suggest that the 1929 earthquake has not influenced the 1968 landslide distribution. Although damage accumulation is specific to landslides in brittle hillslope materials, and not necessarily present in all hillslopes where landslides have been mapped, even if a subset of hillslopes record the legacy of past earthquakes, we should expect to see the signal via this test.

In order to undertake logistic regression analysis, we defined a sample grid at 30 m resolution, based upon a digital elevation model, resampled from the 10 m resolution New Zealand Digital Terrain Model (GNS Science, 2011), using bilinear resampling.

ESURFD
3, 1–52, 2015

Response and predictor variables were then generated for each grid cell. For the response variable, binary grids of landslide-source and non-landslide-source pixels were generated from the mapped 1929 and 1968 landslide source zones. We removed from this analysis the 246 landslides from the 1968 dataset, that occurred as reactivations of 1929 landslide scars, in order to allow our analysis to test exclusively for the influence of hillslope damage accumulation, rather than the effect of slopes over-steepened or undermined by previous landslides. Landslide source areas smaller than the pixel area (900 m^2) were also censored by the resampling and therefore not included in this analysis. Predictor variables (Fig. 10, Table 3) were derived to represent factors previously found to influence landslide occurrence elsewhere (Table 2). For both earthquakes, we used the horizontal distance of each grid cell to the surface projection of the fault (FLD), and the 3-dimensional distance from each grid cell to the closest point on the coseismic fault plane (FPD) as proxies for the regional attenuation of seismic waves and shaking intensity. For the 1968 earthquake, we also used the Shakemap PGA model for this purpose, by interpolating from modelled PGA values at 0.05° (~ 4.5 km) grid spacing (PGA). A binary variable, coding the hanging walls and footwalls (HW), was used to represent hanging wall effects on ground motion. The local hillslope orientation relative to the seismic source (0 for hillslopes with aspect oriented away from the fault rupture, and 1 for aspects oriented towards the fault rupture) was used to represent the incidence angle of seismic waves (HO). Normalised distance from stream to ridge crest (0 for sites located in a stream channel, 1 for sites located on a ridge crest), was used to represent valley-scale patterns of topographic amplification and damping (NDS). Local hillslope gradient, measured over a 90 m spatial window (SL) and two relief metrics (the relief (ER) and SD of elevation within individual drainage basins, divided by the drainage basin area) were used to represent the magnitude of static stresses. A categorical variable indicating different lithologies was used to represent variability in material strength (G). In order to capture the regional distribution of structure on bedrock landslides, we generated a binary variable of dip/anti-dip slopes (DS), by comparing local slope gradient and aspect with the azimuth and dip of recorded

ESURFD
3, 1–52, 2015

structures from the New Zealand QMap dataset (Rattenbury et al., 1998, 2006; Nathan et al., 2002), which was interpolated using Theissen polygons. The northerly component of aspect (cosine of aspect, CA) is used to characterize hillslope-scale variations in received solar radiation, which have been associated with the relative intensity of physical and chemical weathering (Mcfadden et al., 2005). Note that CA = 1 indicates hillslopes facing north, which experience higher levels of Southern Hemisphere solar radiation, while CA = −1 indicates hillslopes facing south. In order to account for the effect of pore water pressure, mean monthly precipitation totals for the period 1950–2000 (Hijmans et al., 2005) were used to estimate antecedent precipitation totals for each grid cell, for the 3 months (PD3) and 6 months (PD6) prior to each earthquake. Note that rainfall records from Karamea (NIWA, 2011), suggest similar levels of rainfall preceded the two events. For example June 1929 received 307 mm (May–June 1929 received 406 mm), and May 1968 received 275 mm (April–May 1968 received 525 mm).

In order to avoid the problem of over-fitting regression models, an issue particularly characteristic of automated fitting procedures (e.g.: Hosmer and Lemeshow, 2000), model fitting was undertaken manually, and based on the following criteria:

1. All predictors must have a logical, statistically significant ($p < 0.05$) and consistent influence on P_{ls} for both earthquakes. Whilst the regression coefficient associated with a variable may differ between the two events, this condition stipulates that the direction of influence (±) must remain constant.

2. Any predictor variable added to the model must improve the fit of the model, as determined by McFadden's Pseudo R^2 (McFadden, 1974):

$$R^2 = 1 - \frac{\ln \hat{L}(M_{\text{full}})}{\ln \hat{L}(M_{\text{intercept}})} \tag{3}$$

where $\ln \hat{L}(M_{\text{full}})$ is the log likelihood of the full model and $\ln \hat{L}(M_{\text{intercept}})$ is the log likelihood of the model without any predictors. Pseudo R^2 values indicate the level of

ESURFD
3, 1–52, 2015

improvement offered by the full model over the model without its predictors. During the fitting process multiple variable combinations were iteratively tested. The final models presented below represent those that produced the best fit whilst meeting the above criteria.

During the model fitting, grid cells with hillslope gradient > 58° were found to produce numerical problems associated with the very low frequency of data at high values. This amounted to an area of 1.3 km^2 (less than 0.05 % of the study area). In this range the relationship between hillslope gradient and failure probability was found to exhibit a rollover, suggesting a decrease in failure probability at high gradients. It is unclear whether this behaviour is real or an artefact of the low data frequency and/or a limitation of mapping landslides on steep slopes from aerial imagery, or a deterioration of the DEM quality at high gradients. As the logistic function cannot model a modal relationship, and as slope gradient this is one of the dominant variables in the model, these cells were removed from the analysis prior to model fitting.

5 Results

5.1 Earthquake-induced hillslope failure probability models

We derived two versions of fitted models to hindcast hillslope failure probability, which differ in their characterisation of the regional distribution of ground motions. For both earthquakes, models were derived using fault plane distance, FPD, as a proxy for ground motion. For the 1968 earthquake we also present a model using PGA in place of FPD, which constrains the landslide distribution more accurately. In our FPD-based model for the 1929 and 1968 earthquakes, hillslope failure probability can be modelled via the following equation:

$$P_{\mathrm{LS}}(A) = \frac{1}{1 - e\left(-\left(\begin{array}{l} c_{\mathrm{intercept}} + c_{\mathrm{FPD}}\mathrm{FPD} + c_{\mathrm{NDS}}\mathrm{NDS} \\ +c_{\mathrm{SL}(G)}\mathrm{SL} + c_{\mathrm{CA}}\mathrm{CA} \end{array}\right)\right)} \quad (4)$$

ESURFD
3, 1–52, 2015

where the regression coefficients are indicated by c. Similarly, in our PGA-based model for the 1968 earthquake, hillslope failure probability can be modelled via the following equation:

$$P_{\mathrm{LS}}(A) = \frac{1}{1 - e\left(-\left(\begin{array}{l} c_{\mathrm{intercept}} + c_{\mathrm{PGA}}\mathrm{PGA} + c_{\mathrm{NDS}}\mathrm{NDS} \\ +c_{\mathrm{SL}(G)}\mathrm{SL} + c_{\mathrm{CA}}\mathrm{CA} \end{array}\right)\right)} \quad (5)$$

The regression coefficients and fit statistics for these models are given in Table 4, while Fig. 11 presents a comparison of predicted and observed P_{LS}.

In each model, landslide probability is expressed as a function of the regional seismic ground motion (characterized by 3-dimensional distance from the fault plane or Shakemap PGA), hillslope gradient (where the influence of hillslope gradient varies with lithology), normalized distance from stream to ridge crest, and the northerly component of slope aspect. Note that the lithology predictor variable has more explanatory power and significance when it is used to allow variability in the effect (coefficient) for hillslope gradient, rather than allowing a categorical lithology variable to modify landslide probability directly. All other variables tested during model fitting were found to be less effective predictors than those included in the models presented, or failed in one or both of the fitting criteria. Note that these models describe the relative spatial distribution of landslides, while absolute differences in the size of the earthquakes are accounted for implicitly by fitting the model separately for each earthquake.

For both model versions, predicted and observed probabilities display a good fit to the line of equality (Fig. 11c). P_{LS} values hindcast using Eq. (4) display a slight overprediction at low probability values. It is likely that these errors at the lower limit of the distribution of probabilities are at least in part statistical artefacts of low data frequency and near-zero probability values. In the case of the 1968 earthquake, P_{LS} values hindcast using Eq. (4) are offset to the east of the mapped foci of landslides (Fig. 11b). This is most likely due to the lack of consideration given to rupture directivity effects when using distance alone as a proxy for ground motion. P_{LS} values hindcast using

ESURFD
3, 1–52, 2015

Eq. (4) do not exhibit this artefact, and provide a better spatial match to the observed landslide distribution. This model also derives a better fit (pseudo-R^2 = 0.246) than Eq. (4) (pseudo-R^2 = 0.208), with no departure from a 1 : 1 relationship at low P_{LS} values (Fig. 11g).

Although each predictor explains a component of the variance in the spatial distribution of failures, not all variables contribute equally. Figure 12 presents the predictor variables in rank order of their importance in each model, determined by sequentially removing the predictor contributing least to the fit of the model. In all three models, the regional ground motion proxy (distance from the fault plane or PGA) and hillslope gradient rank as the top two variables, followed by geology, the NDS topographic amplification proxy, then the hillslope aspect weathering proxy. In all three models, the regional ground motion, hillslope gradient and geology account for over 90 % of the total model fit, while topographic amplification and the relative intensity of hillslope weathering are secondary in defining the spatial distribution of landslides.

5.2 Influence of the 1929 earthquake on the 1968 landslide distribution

To test our hypothesis we use Eq. (5), which most accurately hindcasts the 1968 landslide distribution. Figure 13 presents the results of our analysis in a form equivalent to that outlined conceptually in Fig. 9. When plotted against the predictor variables (Fig. 13a–e), there is no trend in the residuals, which suggests that the model predictors are generally well fitted to the data. However, when plotted by hindcast P_{LS} for the 1929 earthquake ($P_{LS}1929$), the 1968 residuals display a positive trend (Fig. 13g). Hillslopes with $P_{LS}1929$ greater than 0.013 (38 % of the overlap region mapped for both events) exhibit higher P_{LS} in the 1968 earthquake than predicted by Eq. (5) alone. Conversely, P_{LS} in the 1968 earthquake is over-predicted for hillslopes exhibiting $P_{LS}1929$ less than 0.013. The factor driving the difference between the 1968 and 1929 P_{LS} models is the distribution of ground motion. Consequently we find correlation between the residuals and distance from the 1929 seismic source (Fig. 13h). The significance of this relationship can be tested by adding the distance from the 1929 fault (FPD(1929)) into

ESURFD
3, 1–52, 2015

Eq. (5), and refitting the model (Table 5). The results of this regression show that the 1929 regional ground motion yields a significant, negative coefficient. This indicates that once other variables are accounted for, landslide probability in 1968 is higher for hillslopes that experienced strong ground motions in the previous 1929 earthquake.

6 Discussion

Our results both support the findings of previous work into modelling earthquake-induced landslides, as well as providing new insights into how past earthquakes influence future landslide distributions. The roles of individual components in our logistic regression models are in agreement with those observed in previous studies (e.g.: Dai et al., 2011; Meunier et al., 2008, 2007), and the presence of these relationships in both the 1929 and 1968 earthquakes supports the extrapolation of these models both temporally as well as spatially. A number of variables that we might expect to influence the landslide distribution showed no significant influence when the effect of other predictors was controlled for. This particularly concerns factors influencing the aspect of landslides, which implies that patterns observed in other earthquakes may be regionally specific or confounded by the influence of other more "powerful" predictors that might not have been controlled for. The consistency with which the model describes the spatial distribution of hillslope failures for both events suggests that the combination of underlying relationships presented in Eqs. (4) and (5) may be applied more generally to earthquakes in this region. In other words, landslides triggered by earthquakes in this area are likely to be defined by the spatial distribution of hillslope failure probability identified here. By removing the less influential variables and identifying the more major influences on failure probability, the model can be made less event-specific and so more transferrable. The combination of ground motion and local hillslope gradient, with the influence of hillslope gradient dependent on lithology, therefore provides a candidate variable subset for a generalized earthquake-induced landslide probability model.

ESURFD
3, 1–52, 2015

While time-independent variables provide useful constraints on the spatial distribution of landslides, our results suggest that previous earthquakes also impart a significant influence on future landsliding. Residuals in the landslide distribution predicted for the 1968 earthquake suggest that hillslopes with higher predicted P_{ls} in 1929 exhibit higher than expected P_{ls} in 1968. This implies that, despite the widespread failure of unstable hillslopes in 1929, at least some of those hillslopes that did not fail in 1929 were preconditioned and thus were more susceptible to failure in 1968. This behaviour is consistent with our hypothesized influence of damage accumulation, where failure occurred in brittle hillslope materials. Our results suggest that in the case of the 1929 earthquake, damage in unfailed hillslopes persists, resulting in regions close to the 1929 seismic source having enhanced sensitivity to landslide triggering in 1968.

If hillslopes have accrued damage from the 1929 earthquake, then we would also expect them to have accumulated damage from other seismic events, both prior to 1929 and during the intervening 1929–1968 period. It is reasonable to assume that other processes that induce strain-dependent weakening in hillslopes (e.g.: storms, which alter the stress distribution in hillslopes via pore-pressure generation) also drive damage accumulation during interseismic periods. Results from previous investigations suggest that, following large earthquakes, rainfall and smaller seismic events are accompanied by a gradual decay in levels of landslide activity (Hovius et al., 2011; Saba et al., 2010; Tang et al., 2011). In these "smaller" events, removal of damaged material via landsliding, leading to a gradual reduction in landslide susceptibility, appears to dominate. When strong ground motions occur, accumulation of damage appears to dominate, leading an abrupt increase in landslide susceptibility. We can hypothesise a complex overprint of hillslope preconditioning resulting from previous earthquakes and storms, with those more recent, higher magnitude earthquakes exhibiting a stronger influence on the current landslide distribution than less recent, lower magnitude earthquakes and storms. Similarly, the apparently stochastic nature of landslide occurrence and the inability of current models to identify the exact hillslopes that undergo failure may in part result from not knowing the condition of each hillsope at the onset of shaking. If this

ESURFD
3, 1–52, 2015

condition is dependent upon the history of past damage-inducing events, then building historical data, or appropriate proxies, into landslide models may provide a means of reducing some of this uncertainty.

7 Conclusions

The main conclusions drawn from this study can be summarized as follows:

1. The 1929 and 1968 earthquakes reveal a consistent spatial pattern of landslides that can be modelled probabilistically as a function of spatial variability in seismic ground motion, hillslope gradient, lithology, valley-scale topographic amplification and damping, and directional variability in hillslope material weathering. Statistically, the seismic ground motion and hillslope gradient (where the influence of hillslope gradient is lithologically dependent) account for the majority (> 90 %) of the explanatory power of the model. We may therefore conclude that these factors are the most important considerations for predicting an earthquake-induced landslide distribution.

2. Once the influence of known factors influencing landslide occurrence has been controlled for, our results suggest that the legacy of the 1929 Buller earthquake influenced the spatial distribution of landslides triggered by the 1968 Inangahua earthquake. This effect is consistent with the accumulation of damage in hillslopes that did not fail in the 1929 earthquake, where failure occurs in brittle materials. From this result, we hypothesize the importance of overprinting of past seismic, and by implication a-seismic, events which leads to a legacy of material damage influencing susceptibility to future earthquake-triggered landslides.

3. Our findings emphasize that a lack of knowledge of the current damage state of hillslopes in a landscape potentially represents a significant source of uncertainty when assessing landslide susceptibility. This creates the potential for inaccuracy

ESURFD
3, 1–52, 2015

in landslide susceptibility models. A longer-term perspective is necessary if we are to better understand this process and how brittle damage affects the evolution and landslide dynamics of active mountain ranges. Specifically, this requires accurate, multi-temporal mapping of landslide distributions, resampled following individual earthquakes, aftershocks and storms. Spatial–temporal analysis of such data would represent a significant step towards better understanding of temporal correlation between past and future landslide-triggering events. Future work could then explore the value of adding historical and paleo seismic and climatic data into landslide models, providing a means of making susceptibility assessments dynamic through time.

Appendix A: Aerial imagery used for landslide mapping

Details of aerial imagery used for landslide mapping are provided in Table A1 and Fig. A1.

Appendix B: Extraction of landslide source areas

In order to delineate landslide source areas, where the quality of aerial imagery did not allow visual separation of source and runout-deposit areas, we developed a topographic algorithm. Landslide polygons were separated into source and runout-deposit zones, by dividing each landslide along its mid-elevation contour. This process is illustrated in Fig. B1. Comparison of visually- and algorithm-delineated source areas, for a sample of 51 landslides, suggest that this technique provides a reasonable approximation of landslide source areas (Fig. B2.).

Author contributions. G. Hancox initiated studies of the 1929 and 1968 earthquakes and conducted the landslide mapping, which was updated and digitised by R. N. Parker. R. N. Parker and G. Hancox collected field data and prepared the figures. R. N. Parker, N. J. Rosser,

ESURFD
3, 1–52, 2015

D. N. Petley and A. L. Densmore conceived the idea. R. N. Parker conducted the analysis and wrote the paper with input from N. J. Rosser, D. N. Petley., A. L. Densmore, C. Massey and G. Hancox.

Acknowledgements. Funding for this research was provided by the Willis Research Network and GNS Science.

We thank A. Zajac, M. McSaveney, N. Cox, M. Rattenbury, W. Murphy, M. Brain and M. Stirling for their assistance.

References

Abrahamson, N. A. and Somerville, P. G.: Effects of the hanging wall and foot wall on ground motions recorded during the Northridge earthquake, B. Seismol. Soc. Am., 86, S93–S99, 1996.

Abrahamson, N., Atkinson, G., Boore, D., Bozorgnia, Y., Campbell, K., Chiou, B., Idriss, I. M., Silva, W., and Youngs, R.: Comparisons of the NGA ground–motion relations, Earthq. Spectra, 24, 45–66, doi:10.1193/1.2924363, 2008.

Adams, R. D., Eiby, G. A., and Lowry, M. A.: Preliminary reports on the Inangahua earthquake, New Zealand, May 1968: Preliminary seismological report, New Zealand DSIR Bull., 193, 7–16, 1968.

Anderson, H., Webb, T., and Jackson, J.: Focal mechanisms of large earthquakes in the South Island of New Zealand: implications for the accommodation of Pacific-Australia plate motion, Geophys. J. Int., 115, 1032–1054, 1993.

Anderson, H., Beanland, S., Buck, G., Darby, D., Downes, G., Haines, J., Jackson, J., Robinson, R., and Webb, T.: The 1968 23 May Inangahua, New Zealand, earthquake: an integrated geological, geodetic, and seismological source model, New Zeal. J. Geol. Geop., 37, 59–86, 1994.

Benites, R. A., Haines, A. J., New Zealand. Earthquake, C., Institute of, G., and Nuclear Sciences, L.: Quantification of Seismic Wavefield Amplification by Topographic Features, Institute of Geological & Nuclear Science, Wellington, NZ, 1994.

Berryman, K. R.: Late quaternary movement on White Creek Fault, South Island, New Zealand, New Zeal. J. Geol. Geop., 23, 93–101, 1980.

ESURFD

3, 1–52, 2015

Bouchon, M.: Effect of topography on surface motion, B. Seismol. Soc. Am., 63, 615–632, 1973.
Campbell, K. W. and Bozorgnia, Y.: NGA ground motion model for the geometric mean horizontal component of PGA, PGV, PGD and 5 % damped linear elastic response spectra for periods ranging from 0.01 to 10 s, Earthq. Spectra, 24, 139–171, doi:10.1193/1.2857546, 2008.
Capolongo, D., Refice, A., and Mankelow, J.: Evaluating earthquake-triggered landslide hazard at the basin scale through GIS in the Upper Sele river Valley, Symposim on Assessment and Mitigation of Multiple Hazards, Nice, France, ISI:000179499400006, 595–625, 2002.
Chen, X.-Q., Li, Y., Gao, Q., and Jia, S.-T.: Distribution characteristics of geo-hazards in Ganxi Valley after the Wenchuan earthquake, Environ. Earth Sci., 65, 965–973, doi:10.1007/s12665-011-1018-8, 2012.
Clarke, B. A. and Burbank, D. W.: Quantifying bedrock-fracture patterns within the shallow subsurface: implications for rock mass strength, bedrock landslides, and erodibility, J. Geophys. Res.-Earth, 116, F04009, doi:10.1029/2011jf001987, 2011.
Clauset, A., Shalizi, C. R., and Newman, M. E. J.: Power-law distributions in empirical data, SIAM Rev., 51, 661–703, doi:10.1137/070710111, 2009.
Cox, D. R.: Regression analysis of binary sequences (with discussion), J. Roy. Stat. Soc. B, 20, 215–242, 1958.
Dai, F. C. and Lee, C. F.: A spatiotemporal probabilistic modelling of storm-induced shallow landsliding using aerial photographs and logistic regression, Earth Surf. Proc. Land., 28, 527–545, 2003.
Dai, F. C., Xu, C., Yao, X., Xu, L., Tu, X. B., and Gong, Q. M.: Spatial distribution of landslides triggered by the 2008 M_s 8.0 Wenchuan earthquake, China, J. Asian Earth Sci., 40, 883–895, doi:10.1016/j.jseaes.2010.04.010, 2011.
Davis, L. L. and West, L. R.: Observed effects of topography on ground motion, B. Seismol. Soc. Am., 63, 283–298, 1973.
Dellow, G. D. and Hancox, G. T.: The influence of rainfall on earthquake-induced landslides in New Zealand, in: Proceedings of Technical Groups, Earthquakes and Urban Development: New Zealand Geotechnical Society 2006 Symposium, Nelson, New Zealand, 355–368, 2006.
Densmore, A. L., Anderson, R. S., McAdoo, B. G., and Ellis, M. A.: Hillslope evolution by bedrock landslides, Science, 275, 369–372, doi:10.1126/science.275.5298.369, 1997.

ESURFD
3, 1–52, 2015

Doser, D. I., Webb, T. H., and Maunder, D. E.: Source parameters of large historical (1918–1962) earthquakes, South Island, New Zealand, Geophys. J. Int., 139, 769–794, 1999.
Dowrick, D. J.: Damage and intensities in the magnitude 7.8 1929 Murchison, New Zealand, Earthquake, Bull. N. Z. Nat. Soc. Earthquake Eng., 27, 190–204, 1994.
Dowrick, D. J. and Rhoades, D. A.: Magnitudes of New Zealand earthquakes, 1901–1993, Bull. N. Z. Nat. Soc. Earthq. Eng., 31, 260–280, 1998.
Dowrick, D. J. and Sritharan, S.: Peak ground accelerations recorded in the 1968 Inangahua earthquake and some implications, Bull. N. Z. Nat. Soc. Earthq. Eng., 26, 349–355, 1993.
Evans, B., Fredrich, J. T., and Wong, T.-F.: The Brittle-Ductile Transition in rocks: recent experimental and theoretical progress, in: The Brittle-Ductile Transition in Rocks, American Geophysical Union, 1–20, 2013.
Fyfe, H. E.: Movement of the White Creek Fault, New Zealand, N. Z. J. Sci. Tech., 11, 192–197, 1929.
Garcia-Rodriguez, M. J., Malpica, J. A., Benito, B., and Diaz, M.: Susceptibility assessment of earthquake-triggered landslides in El Salvador using logistic regression, Geomorphology, 95, 172–191, doi:10.1016/j.geomorph.2007.06.001, 2008.
Guzzetti, F., Malamud, B. D., Turcotte, D. L., and Reichenbach, P.: Power-law correlations of landslide areas in central Italy, Earth Planet. Sc. Lett., 195, 169–183, 2002.
Haines, J.: 1929 Murchison Earthquake, Neotectonics of the Buller Region Workshop, Department of Scientific and Industrial Research Geology and Geophysics, Wellington, New Zealand, 1991.
Hancox, G. T., Perrin, N. D., and Dellow, G. D.: Earthquake-induced landsliding in New Zealand and implications for MM intensity and seismic hazard assessment, GNS Client Report 43601B, Lower Hutt, New Zealand, 1997.
Hancox, G. T., Perrin, N. D., and Dellow, G. D.: Recent studies of historical earthquake-induced landsliding, ground damage, and MM intensity in New Zealand, Bu. NZ Nat. Soc. Earthq. Eng., 35, 59–95, 2002.
Hancox, G. T., Ries, W., Lukovic, B., and Parker, R.: Landslides and ground damage caused by the Mw 7.1 Inangahua Earthquake of 24th May 1968 in north west South Island, New Zealand, GNS Science Report 2014/06, 89, Lower Hutt, New Zealand, 2014.
Henderson, J.: The west Nelson earthquakes of 1929 (with Notes on the Geological Structure of West Nelson), The New Zealand J. Sci. Technol., XIX, 66–144, 1937.

ESURFD
3, 1–52, 2015

Hijmans, R. J., Cameron, S. E., Parra, J. L., Jones, P. G., and Jarvis, A.: Very high resolution interpolated climate surfaces for global land areas, Int. J. Climatol., 25, 1965–1978, 2005.
Hoek, E., Carranza-Torres, C., and Corkum, B.: Hoek–Brown Failure Criterion – 2002 Edition, NARMS-TAC Conference, 7–10 July 2002, Toronto, 267–273, 2002.
Hosmer, D. W. and Lemeshow, S.: Applied Logistic Regression, 2 edn., John Wiley & Sons Inc., New York, 2000.
Hovius, N., Stark, C. P., and Allen, P. A.: Sediment flux from a mountain belt derived by landslide mapping, Geology, 25, 231–234, 1997.
Hovius, N., Meunier, P., Lin, C.-W., Chen, H., Chen, Y.-G., Dadson, S., Horng, M.-J., and Lines, M.: Prolonged seismically induced erosion and the mass balance of a large earthquake, Earth Planet. Sc. Lett., 304, 347–355, doi:10.1016/j.epsl.2011.02.005, 2011.
Hungr, O., Leroueil, S., and Picarelli, L.: The Varnes classification of landslide types, an update, Landslides, 11, 167–194, doi:10.1007/s10346-013-0436-y, 2014.
Iverson, R. M.: Landslide triggering by rain infiltration, Water Resour. Res., 36, 1897–1910, 2000.
Jibson, R. W., Harp, E. L., and Michael, J. A.: A method for producing digital probabilistic seismic landslide hazard maps, Eng. Geol., 58, 271–289, 2000.
Jibson, R. W.: Methods for assessing the stability of slopes during earthquakes – a retrospective, Eng. Geol., 122, 43–50, doi:10.1016/j.enggeo.2010.09.017, 2011.
Keefer, D. K.: Landslides caused by earthquakes, Geol. Soc. Am. Bull., 95, 406–421, 1984.
Keefer, D. K.: Statistical analysis of an earthquake-induced landslide distribution – the 1989 Loma Prieta, California event, Eng. Geol., 58, 231–249, 2000.
Keefer, D. K.: Investigating landslides caused by earthquakes – a historical review, Surv. Geophys., 23, 473–510, 2002.
Khazai, B. and Sitar, N.: Evaluation of factors controlling earthquake-induced landslides caused by Chi-Chi earthquake and comparison with the Northridge and Loma Prieta events, Eng. Geol., 71, 79–95, 2004.
Lee, C.-T., Huang, C.-C., Lee, J.-F., Pan, K. -L., Lin, M.-L., and Dong, J.-J.: Statistical approach to storm event-induced landslides susceptibility, Nat. Hazards Earth Syst. Sci., 8, 941–960, doi:10.5194/nhess-8-941-2008, 2008.
Lee, S. T., Yu, T. T., and Peng, W. F.: Effect of earthquake on subsequent typhoon-induced landslides using remote sensing imagery in the 99 peaks region, central Taiwan, Key Eng. Mat., 500, 773–779, 2012.

ESURFD
3, 1–52, 2015

Lensen, G. J. and Suggate, R. P.: Inangahua earthquake-preliminary account of geology, in: Preliminary Reports on the Inangahua Earthquake, New Zealand, May 1968, edited by: Adams, R. D., Eiby, G. A., Lowry, M. A., Lensen, G. J., Suggate, R. P., and Stephenson, W. R.: New Zealand Department of Scientific and Industrial Research Bulletin, Wellington, New Zealand, 17–36, 1968.

Leroueil, S., Locat, A., Eberhardt, E., and Kovacevic, N.: Progressive failure in natural and engineered slopes, in: Landslides and Engineered Slopes, edited by: Eberhardt, E., Froese, C., Turner, A. K., and Leroueil, S., Taylor & Francis Group, London, 31–46, 2012.

Li, G., West, A. J., Densmore, A. L., Jin, Z., Parker, R. N., and Hilton, R. G.: Seismic mountain building: landslides associated with the 2008 Wenchuan earthquake in the context of a generalized model for earthquake volume balance, Geochem. Geophy. Geosy., 15, 833–844, doi:10.1002/2013GC005067, 2014.

Liu, J. K., Wong, C. C., Huang, J. J., and Yang, M. J.: Landslide enhancement images for the study of torrential rainfall landslides, Proceeding of the 23rd Asian conference on Remote Sensing, 25–29 November 2002, Kathmandu, 193–198, 2002.

Malamud, B. D., Turcotte, D. L., Guzzetti, F., and Reichenbach, P.: Landslides, earthquakes, and erosion, Earth Planet. Sc. Lett., 229, 45–59, doi:10.1016/j.epsl.2004.10.018, 2004.

Massey, C. I., Della Pasqua, F., Taig, T., Lukovic, B., Ries, W., Heron, D., and Archibald, G.: Canterbury Earthquakes 2010/11 Port Hills Slope Stability: Risk assessment for Redcliffs, GNS Science, Wellington, New Zealand, p. 123 + Appendices, 2014a.

Massey, C. I., Taig, T., Della Pasqua, F., Lukovic, B., Ries, W., and Archibald, G.: Canterbury Earthquakes 2010/11 Port Hills Slope Stability: Debris avalanche risk assessment for Richmond Hill, GNS Science, Wellington, New Zealand, p. 132 + Appendices, 2014b.

Mcfadden, L. D., Eppes, M. C., Gillespie, A. R., and Hallet, B.: Physical weathering in arid landscapes due to diurnal variation in the direction of solar heating, Bull. Geol. Soc. Am., 117, 161–173, 2005.

Meunier, P., Hovius, N., and Haines, J.: Regional patterns of earthquake-triggered landslides and their relation to ground motion, Geophys. Res. Lett., 34, 1–5, 2007.

Meunier, P., Hovius, N., and Haines, J. A.: Topographic site effects and the location of earthquake induced landslides, Earth Planet. Sc. Lett., 275, 221–232, 2008.

Meunier, P., Uchida, T., and Hovius, N.: Landslide patterns reveal the sources of large earthquakes, Earth Planet. Sc. Lett., 363, 27–33, doi:10.1016/j.epsl.2012.12.018, 2013.

ESURFD

3, 1–52, 2015

Moore, J. R., Sanders, J. W., Dietrich, W. E., and Glaser, S. D.: Influence of rock mass strength on the erosion rate of alpine cliffs, Earth Surf. Proc. Land., 34, 1339–1352, 2009.
Nathan, S., Rattenbury, M. S., and Suggate, R. P.: Geology of the Greymouth Area, Institute of Geological & Nuclear Sciences 1 : 250 000 Geological Map 12, GNS Science, Lower Hutt, New Zealand, 2002.
Newmark, N. M.: Effects of earthquakes on dams and embankments, Geotechnique, 15, 139–159, 1965.
Nichol, J. and Wong, M. S.: Satellite remote sensing for detailed landslide inventories using change detection and image fusion, Int. J. Remote Sens., 26, 1913–1926, doi:10.1080/01431160512331314047, 2005.
Parise, M. and Jibson, R. W.: A seismic landslide susceptibility rating of geologic units based on analysis of characteristics of landslides triggered by the 17 January 1994 Northridge, California earthquake, Eng. Geol., 58, 251–270, 2000.
Parker, R. N.: Controls on the Distribution of Landslides Triggered by the 2008 Wenchuan Earthquake, Sichuan Province, China, M.S. thesis, Institute of Hazard Risk and Resilience, Department of Geography, University of Durham, Durham, 2010.
Parker, R. N.: Hillslope Memory and Spatial and Temporal Distributions of Earthquake-Induced Landslides, PhD thesis, Department of Geography, Durham University, Durham, UK, 2013.
Pearce, A. J. and O'Loughin, C. L.: Landsliding during a *M* 7.7 earthquake: influence of geology and topography, Geology, 13, 855–858, 1985.
Perrin, N. D. and Hancox, G. T.: Landslide-dammed lakes in New Zealand, Proceedings of the Sixth International Symposium on Landslides, Christchurch, 10–14 February 1992, 1457–1466, 1992.
Petley, D. N. and Allison, R. J.: The mechanics of deep-seated landslides, Earth Surf. Proc. Land., 22, 747–758, doi:10.1002/(sici)1096-9837(199708)22:8<747:aid-esp767>3.0.co;2-#, 1997.
Petley, D. N., Higuchi, T., Petley, D. J., Bulmer, M. H., and Carey, J.: Development of progressive landslide failure in cohesive materials, Geology, 33, 201–204, doi:10.1130/g21147.1, 2005.
Rattenbury, M. S., Cooper, R., and Johnston, M. R.: Geology of the Nelson Area, Institute of Geological & Nuclear Sciences 1 : 250 000 Geological Map 9, GNS Science, Lower Hull, New Zealand, 1998.

ESURFD
3, 1–52, 2015

Rattenbury, M. S., Townsend, D. B., and Johnston, M. R.: Geology of the Kaikoura Area, Institute of Geological & Nuclear Sciences 1 : 250 000 Geological Map 13, GNS Science, Lower Hutt, New Zealand, 2006.

Saba, S. B., van der Meijde, M., and van der Werff, H.: Spatiotemporal landslide detection for the 2005 Kashmir earthquake region, Geomorphology, 124, 17–25, doi:10.1016/j.geomorph.2010.07.026, 2010.

Selby, M. J.: Hillslope Materials and Processes, Oxford University Press, Oxford, UK, 451 pp., 2005.

Somerville, P. G., Smith, N. F., Graves, R. W., and Abrahamson, N. A.: Modification of empirical strong ground motion attenuation relations to include the amplitude and duration effects of rupture directivity, B. Seismol. Soc. Am., 68, 199–222, 1997.

Stark, C. P. and Guzzetti, F.: Landslide rupture and the probability distribution of mobilized debris volumes, J. Geophys. Res.-Earth, 114, 1–16, F00a02, doi:10.1029/2008jf001008, 2009.

Stirling, M. W., McVerry, G., Berryman, K. R., McGinty, P., Villamor, P., Van Dissen, R., Dowrick, D. J., and Cousins, J.: Probabilistic seismic hazard assessment of New Zealand, prepared for Earthquake Commission Research Foundation, Institute of Geological and Nuclear Sciences Ltd, Lower Hutt, New Zealand, Client Report 1999/53, 2000.

Stirling, M. W., Verry, G. H. M., and Berryman, K. R.: A new seismic hazard model for New Zealand, B. Seismol. Soc. Am., 92, 1878–1903, doi:10.1785/0120010156, 2002.

Stirling, M., Litchfield, N., Smith, W., Barnes, P., Gerstenberger, M., McVerry, G., and Pettinga, J.: Updated Probabilistic Seismic Hazard Assessment For the Canterbury Region, GNS Science Consultancy Report 2007/232 – ECan Report Number U06/6, Wellington, New Zealand, 2007.

Stirling, M., McVerry, G., Gerstenberger, M., Litchfield, N., Dissen, R. V., Berryman, K., Barnes, P., Wallace, L., Bradley, B., Villamor, P., Langridge, R., Lamarche, G., Nodder, S., Reyners, M., Rhoades, D., Smith, W., Nicol, A., Pettinga, J., Clark, K., and Jacobs., K.: National seismic hazard model for New Zealand: 2010 update, B. Seismol. Soc. Am., 102, 1514–1542, 2012.

Tang, C., Zhu, J., Qi, X., and Ding, J.: Landslides induced by the Wenchuan earthquake and the subsequent strong rainfall event: a case study in the Beichuan area of China, Eng. Geol., 122, 22–33, doi:10.1016/j.enggeo.2011.03.013, 2011.

USGS: Advanced National Seismic System (ANSS), ShakeMap, Global Region, Maps of Ground Shaking and Intensity For Event 196805231724, Inangahua, New Zealand, 2014.

ESURFD
3, 1–52, 2015

Van Den Eeckhaut, M., Poesen, J., Govers, G., Verstraeten, G., and Demoulin, A.: Characteristics of the size distribution of recent and historical landslides in a populated hilly region, Earth Planet. Sc. Lett., 256, 588–603, doi:10.1016/j.epsl.2007.01.040, 2007.

Varnes, D. J.: Transportation Research Board Special Report: Slope movement types and processes, in: Landslides, Analysis and Control, edited by: Schuster, R. L., and Krizek, R. J., National Academy of Sciences, Washington D.C., USA, 11–33, 1978.

von Ruette, J., Papritz, A., Lehmann, P., Rickli, C., and Or, D.: Spatial statistical modeling of shallow landslides-Validating predictions for different landslide inventories and rainfall events, Geomorphology, 133, 11–22, doi:10.1016/j.geomorph.2011.06.010, 2011.

Walker, S. H. and Duncan, D. B.: Estimation of the probability of an event as a function of several independent variables, Biometrika, 54, 167–178, 1967.

Wu, F. C., Xu, J. Q., Zhao, X. L., and Hu, W. N.: An observed effect of topography on surface motion, Acta Geophys. Sinica, 33, 188–195, 1990.

Yesilnacar, E. and Topal, T.: Landslide susceptibility mapping: a comparison of logistic regression and neural networks methods in a medium scale study, Hendek region (Turkey), Eng. Geol., 79, 251–266, doi:10.1016/j.enggeo.2005.02.002, 2005.

ESURFD

3, 1–52, 2015

Table 1. Summary of 1929 and 1968 earthquakes.

Name	Date	Epicentre Location	Magnitude	Focal depth	Rupture length	Strike	Dip	Dip direction
Buller earthquake	17 Jun 1929	41.70° S, 172.20° E	M_s = 7.8 M_w = 7.7	9 ± 3 km	50 km	15°	45°	100°
Inangahua earthquake	24 May 1968	41.76° S, 171.96° E	M_s = 7.4 M_w = 7.1	10 ± 5 km	30 km	25°	45°	295°

ESURFD
3, 1–52, 2015

Table 2. Summary of proxy variables suggested to influence spatial distributions of earthquake-induced landslides, based on empirical studies.

Proxy variable	Mechanistic link to landslide occurrence	References
	Seismic forcing (Ground motion intensity)	
Seismic wave attributes (e.g., PGA, PGV, PGD, Arias Intensity, MMI)	Local metric of shaking intensity	Meunier et al. (2007, 2013); Dai et al. (2011); Lee et al. (2008);
Distance from the seismic source	Regional attenuation of seismic wave amplitudes	Hancox et al. (1997, 2002)
Position on hillslope (normalised distance from stream to ridge crest)	Ridge to stream patterns of topographic amplification and damping	Davis and West (1973); Bouchon (1973); Wu et al. (1990); Benites et al. (1994); Meunier et al. (2008); Densmore et al. (1997)
Orientation of hillslope relative to seismic source	Directional patterns of topographic amplification and damping, due to the incidence angle of seismic waves	
Hanging wall vs. footwall location of sites	Proximity of the fault and enhanced rupture directivity effects in hanging wall areas	Abrahamson and Somerville (1996); Somerville et al. (1997); Abrahamson et al. (2008)
	Strength of hillslope materials	
Bedrock lithology	Hillslope material strength	Khazai and Sitar (2004); Parise and Jibson (2000); Keefer (2000); Dai et al. (2011)
Structural geology (discontinuities)	Kinematic feasibility, i.e. orientation of bedrock discontinuities relative to slope aspect and topography	Hoek et al. (2002); Selby (2005); Moore et al. (2009)
Northness component of hillslope aspect	Relative intensity of rock breakdown via physical and chemical weathering	Meunier et al. (2008); Parker (2010, 2013); Chen et al. (2012)
Rainfall	The effect of pore water pressure in reducing hillslope effective stress	Dellow and Hancox (2006); Iverson (2000)
	Static stress loading in hillslopes	
Hilllope gradient	Magnitude of static stress	Keefer (2000); Khazai and Sitar (2004);
Local hillslope relief	loading in hillslopes	Lee et al. (2008); Dai et al. (2011)

ESURFD
3, 1–52, 2015

Table 3. Potential predictor variables, ID codes, descriptions and units.

Variable ID	Description	Units
FLD-1929	Horizontal distance of each sample cell to the surface projection of the 1929 fault	km
FPD-1929	3-dimensional distance from each sample cell to the closest point on the 1929 coseismic fault plane	km
HW-1929	Binary variable coding the 1929 hangingwall and footwall	
HO-1929	Local hillslope orientation relative to the 1929 seismic source (incidence angle of seismic waves)	°
FLD-1968	Horizontal distance of each sample cell to the surface projection of the 1968 fault	km
FPD-1968	3-dimensional distance from each sample cell to the closest point on the 1968 coseismic fault plane	km
HW-1968	Binary variable coding the 1968 hangingwall and footwall	
HO-1968	Local hillslope orientation relative to the 1968 seismic source (incidence angle of seismic waves)	°
PGA-1968	Shakemap Peak Ground Acceleration for the 1968 earthquake	g
NDS	Normalised distance from stream to ridge crest	
G	Lithology (tectnostratigraphic terrane units); B – Buller Terrane, I – Igneous intrusives, PQS – Pre-quaternary sediments, QS – Quaternary sediments, T – Takaka Terrane	
SL	Local hillslope gradient	°
ES	SD of elevation within individual drainage basins, divided by the drainage basin area	$m\,m^{-2}$
ER	Range of elevation within individual drainage basins, divided by the drainage basin area	$m\,m^{-2}$
DS	Binary variable of dip-slopes and anti-dipslopes	
CA	Cosine transformation of hillslope aspect (hillslope-scale variations in solar radiation)	
PD3	Long-term mean antecedent precipitation total for 3 months prior to the earthquake	mm
PD6	Long-term mean antecedent precipitation total for 6 months prior to the earthquake	mm

ESURFD
3, 1–52, 2015

Table 4. Logistic regression output coefficients and fit statics.

1929 Buller Earthquake					
Number of observations		4 669 997			
Likelihood ratio chi^2		-3.56×10^5			
Model p value		0.00			
Pseudo R^2		0.183		95 % confidence interval	
Variable	Coefficient	Standard error	p value	Lower bound	Upper bound
FPD	−0.0916	0.0006	0.00	−0.0927	−0.0905
NDS	1.4595	0.015	0.00	1.4302	1.4888
SL(G = 1)	0.0928	0.0004	0.00	0.092	0.0937
SL(G = 2)	0.0815	0.0004	0.00	0.0807	0.0822
SL(G = 3)	0.1099	0.0004	0.00	0.1091	0.1107
SL(G = 4)	0.1348	0.0008	0.00	0.1331	0.1364
CA	0.1117	0.0052	0.00	0.1014	0.1219
Intercept	−6.6782	0.0178	0.00	−6.7132	−6.6433
1968 Inangahua Earthquake					
Number of observations		3 181 861			
Likelihood ratio chi^2		-5.51×10^4			
Model p value		0.00			
Pseudo R^2		0.208		95 % confidence interval	
Variable	Coefficient	Standard error	p value	Lower bound	Upper bound
FPD	−0.2031	0.0018	0.00	−0.2067	−0.1995
NDS	1.0153	0.0404	0.00	0.9361	1.0945
SL(G = 1)	0.0777	0.0011	0.00	0.0755	0.08
SL(G = 2)	0.0822	0.001	0.00	0.0802	0.0842
SL(G = 3)	0.1142	0.0011	0.00	0.112	0.1163
SL(G = 4)	0.1297	0.002	0.00	0.1258	0.1337
CA	0.0987	0.0145	0.00	0.0702	0.1271
Intercept	−6.363	0.0435	0.00	−6.4482	−6.2778
1968 Inangahua Earthquake					
Number of observations		3 181 861			
Likelihood ratio chi^2		-5.24×10^4			
Model p value		0.00			
Pseudo R^2		0.246		95 % confidence interval	
Variable	Coefficient	Standard error	p value	Lower bound	Upper bound
PGA	10.9946	0.0973	0.00	10.804	11.1852
NDS	1.114	0.0413	0.00	1.0331	1.1949
SL(G = 1)	0.099	0.0012	0.00	0.0968	0.1013
SL(G = 2)	0.1082	0.001	0.00	0.1061	0.1102
SL(G = 3)	0.1056	0.0011	0.00	0.1034	0.1077
SL(G = 4)	0.1501	0.0021	0.00	0.146	0.1542
CA	0.1192	0.0146	0.00	0.0906	0.1478
Intercept	−7.0207	0.0418	0.00	−7.1027	−6.9387

ESURFD
3, 1–52, 2015

Table 5. Logistic regression output coefficients and fit statics, for model including the influence of the 1929 earthquake on the 1968 landslide distribution.

1968 Inangahua Earthquake					
Number of observations		3 181 861			
Likelihood ratio chi^2		-5.24×10^4			
Model p value		0.00			
Pseudo R^2		0.247		95 % confidence interval	
Variable	Coefficient	Standard error	p value	Lower bound	Upper bound
$\log_{10}$ PGA (1968)	11.0954	0.094	0.00	10.9112	11.2796
NDS	1.1272	0.0415	0.00	1.0458	1.2085
SL(G = 1)	0.101	0.0012	0.00	0.0987	0.1033
SL(G = 2)	0.1105	0.0011	0.00	0.1084	0.1126
SL(G = 3)	0.1102	0.0011	0.00	0.108	0.1123
SL(G = 4)	0.1504	0.0021	0.00	0.1462	0.1545
CA	0.1188	0.0146	0.00	0.0902	0.1474
FPD (1929)	−0.026	0.0011	0.00	−0.0283	−0.0238
Intercept	−6.6122	0.0457	0.00	−6.7017	−6.5227

ESURFD
3, 1–52, 2015

Table A1. Source and details of imagery used for landslide mapping for the 1929 and 1968 earthquakes.

Source: New Zealand Aerial Mapping (http://www.nzam.com/)
Imagery for mapping of 1929 Buller earthquake-triggered landslides
Survey Number: SN 2033, Feb 1968 Contact Print Scale: 1 : 86 000 Run 4029 Photos 9–56 Run 4030 Photos 6–66 Run 4031 Photos 68–85 Run 4032 Photos 15–38 Run 4033 Photos 18–31
Imagery for mapping of 1968 Inangahua earthquake-triggered landslides
Survey Number: SN 3777 Acquisition period: Nov 1974 Contact Print Scale: 1 : 60 000 Run A-Photos 1–7 Run B-Photos 1–7 Run C-Photos 1–9 Run D-Photos 1–9 Run E-Photos 1–10 Run F-Photos 4–6 Run G-Photos 4–10 Run H-Photos 6–12 Run I-Photos 9–12 Run J-Photos 7–11

ESURFD
3, 1–52, 2015

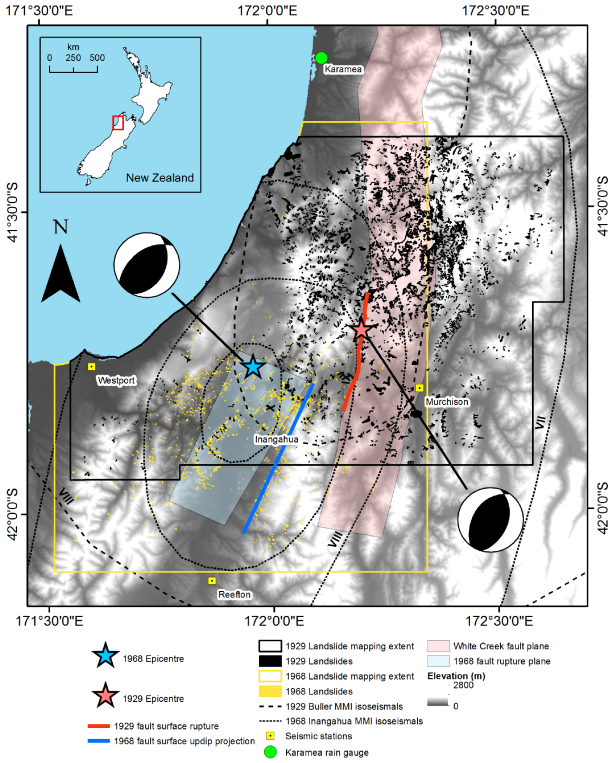

Figure 1. Elevation map of the Buller River to Karamea area of northwest Nelson showing the sources, ground motions and landslides triggered by the 1929 Buller and 1968 Inangahua earthquakes. Included on this map are the epicentres, focal mechanisms and fault planes of the earthquakes (Anderson et al., 1994; Anderson et al., 1993; Stirling et al., 2007), isoseismal contours (Dowrick, 1994; Adams et al., 1968), mapping coverage regions and earthquake-induced landslides mapped in this study.

ESURFD
3, 1–52, 2015

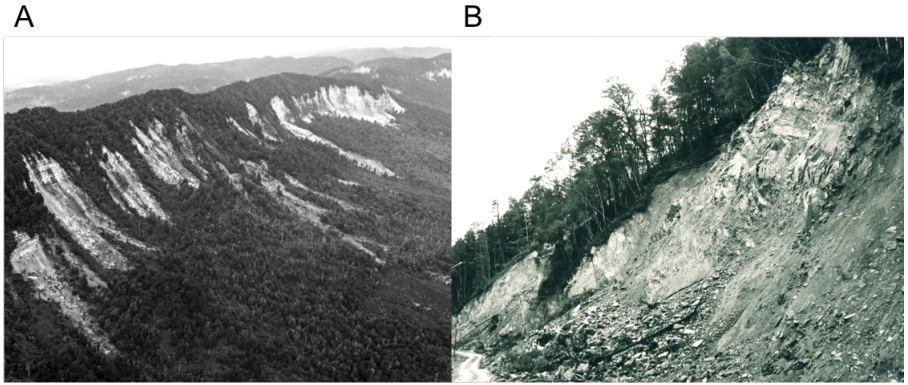

Figure 2. (a) Rock falls from tertiary limestone bluffs at White Cliffs Escarpment, on the south side of the Buller River, 5 km west of Inangahua. **(b)** Rock and debris fall area in the upper Buller Gorge.

ESURFD
3, 1–52, 2015

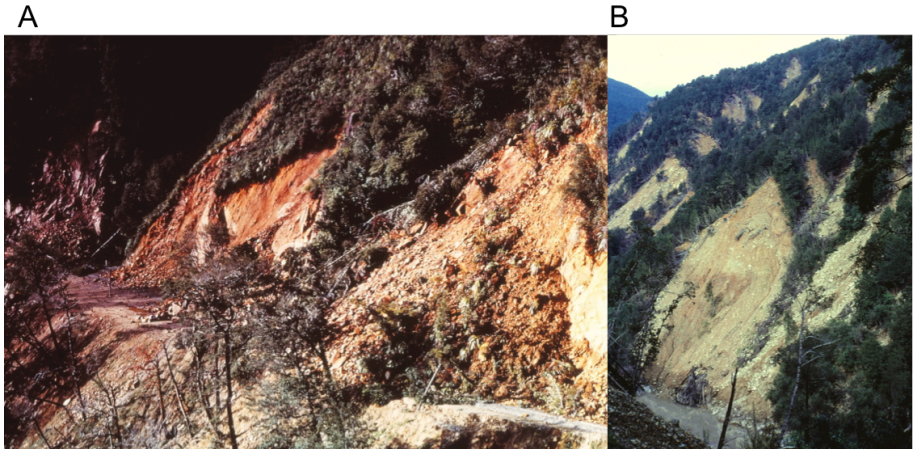

Figure 3. (a) 1968 debris slide on road cut in the upper Buller Gorge. **(b)** Multiple 1968 debris slides on slopes on the south side of the Buller River.

ESURFD
3, 1–52, 2015

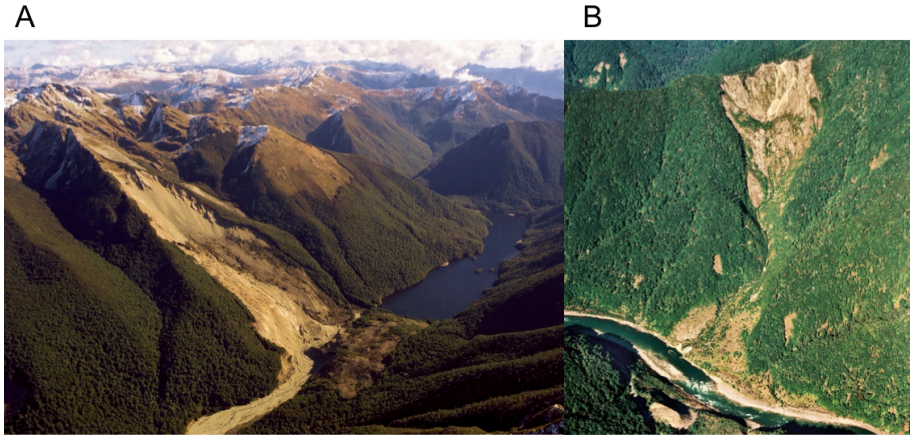

Figure 4. (a) Lake Stanley rock avalanche. The lake was dammed by the landslide, which was trigger by the 1929 earthquake. **(b)** 1995 photo of a rock avalanche that dammed the Buller River during the 1968 earthquake. Apart from vegetation growth, the scar has changed little in the last 40 years.

ESURFD
3, 1–52, 2015

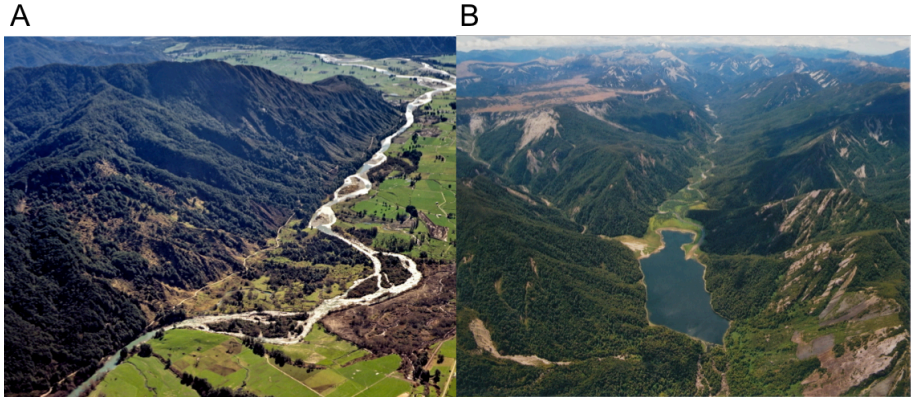

Figure 5. (a) Matakitaki Landslide triggered by the 1929 Earthquake. Debris from this large (18 million m^3) dip-slope rockslide travelled ~ 1 km across the valley floor, killing four people and forming a landslide dam. Note that after over 70 years, the landslide scar is still visible. **(b)** Aerial view of the Matiri Valley (15 km north of Murchison), which was extensively damaged by landslides during the 1929 earthquake. Numerous scars of rockfall and debris slides are still clearly visible in 2011.

ESURFD
3, 1–52, 2015

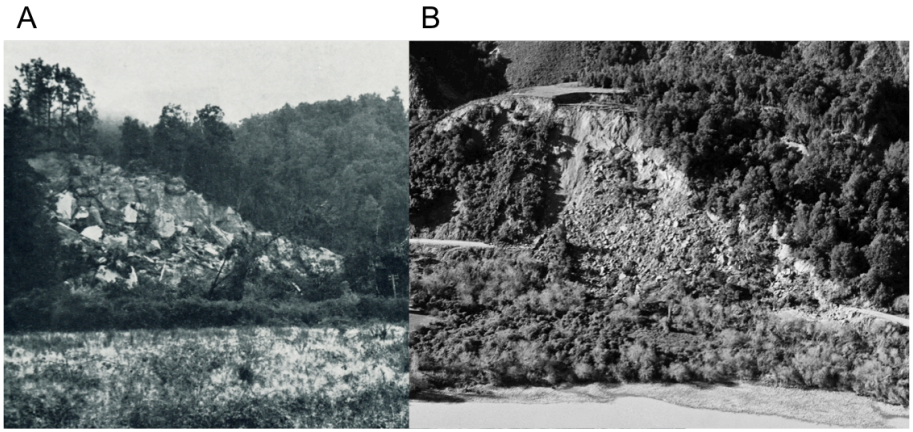

Figure 6. (a) 1968 Oweka Rock Slide with rock debris left (Lensen and Suggate, 1968). **(b)** 1968 rotational slide of ~ 2 million m^3 in sandy ("Blue Bottom") mudstone. At the top of the landslide the semi-intact block below the prominent headscarp has slumped about 6 m. The main body of the slide has carried the rock downslope and comprises highly disrupted mudstone boulders and finer debris.

ESURFD
3, 1–52, 2015

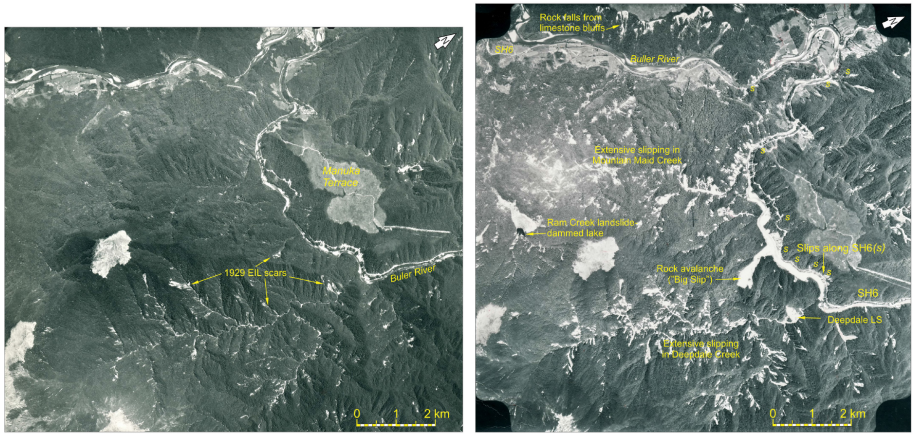

Aerial Photo: Survey No. 2033 - Photo 4031/75 (25 February 1968)

Aerial Photo: Survey No. 3777 - Photo G8 (November 1974)

Figure 7. Two aerial images used to map landslides triggered by the 1929 and 1968 earthquakes in the Buller Gorge area. Scars from the 1929 landslides are recognizable on the SN2033 image (left), 39 years after the earthquake, and many scars were reactivated or enlarged by the 1968 earthquake.

ESURFD
3, 1–52, 2015

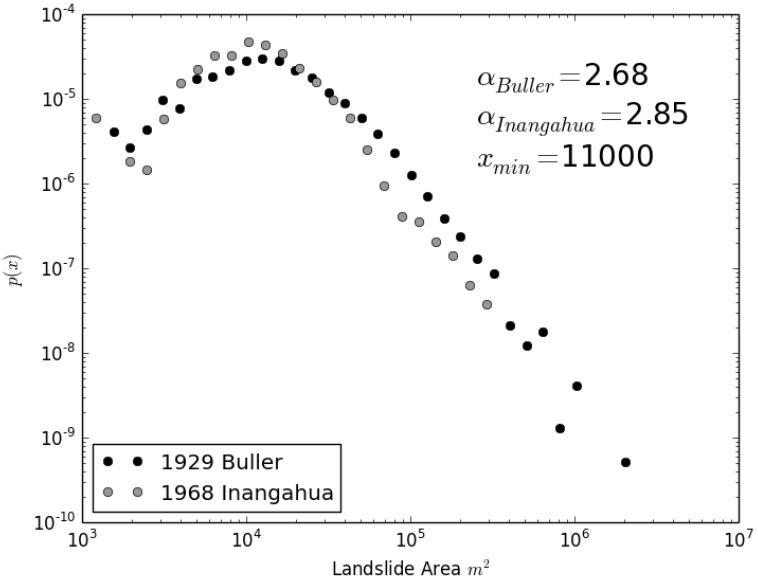

Figure 8. Landslide frequency density as a function of landslide area for the 1929 Buller and 1968 Inangahua earthquake landslide inventories. Data points represent the frequency-density (frequency divided by bin size calculated across logarithmically-spaced bins, after Malamud et al. (2004)). Power-law scaling exponents (α) have been derived using the method of Clauset et al. (2009), for A > 11 000 m^2.

ESURFD
3, 1–52, 2015

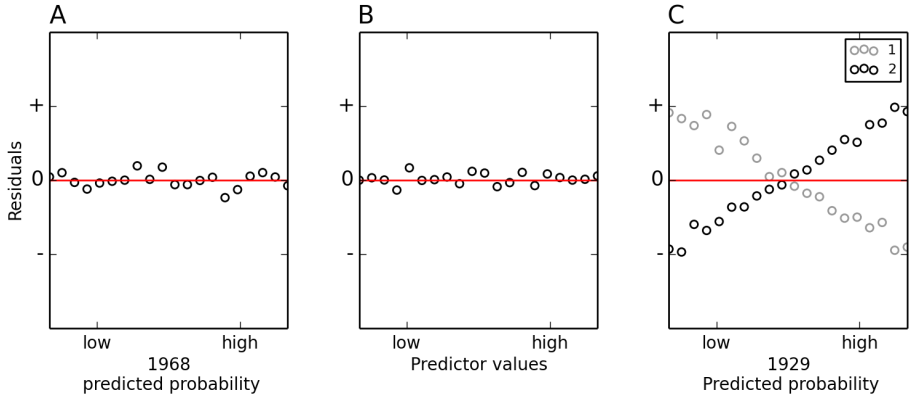

Figure 9. Hypothetical output of hillslope failure conditional probability analysis for the 1929 and 1968 earthquakes. This illustrates how the model residuals (observed P_{ls} minus predicted P_{ls}) would be distributed, if conditional probability models, which account for the full subset of spatial, time-independent factors (i.e.: those not associated with previous events) influencing landslide occurrence, have been fitted and used to hindcast P_{ls}. **(a)** 1968 model residuals are uncorrelated with predicted P_{ls}. **(b)** Model residuals are uncorrelated with values of individual model predictors, **(c)** Model residuals are correlated with P_{ls} hindcast for the 1929 earthquake either negatively (model 1) – indicating preconditioning of hillslopes against failure – or positively (model 2) – indicating preconditioning of hillslopes for failure. Note that residuals are calculated by aggregating probabilities across equal quantile bins of the x variable.

ESURFD
3, 1–52, 2015

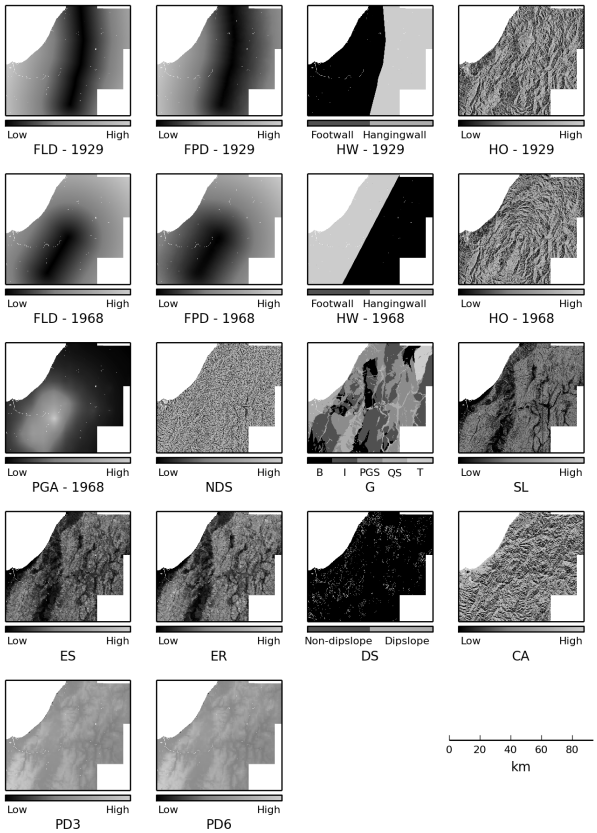

Figure 10. Matrix of maps showing potential predictor variables used in logistic regression analysis of hillslope failure probability. Each map shows distributed values of each predictor variable across the 5629 km^2 combined area of landslide mapping for both events (as shown in Fig. 1). Variable descriptors and units are summarised in Table 3.

ESURFD
3, 1–52, 2015

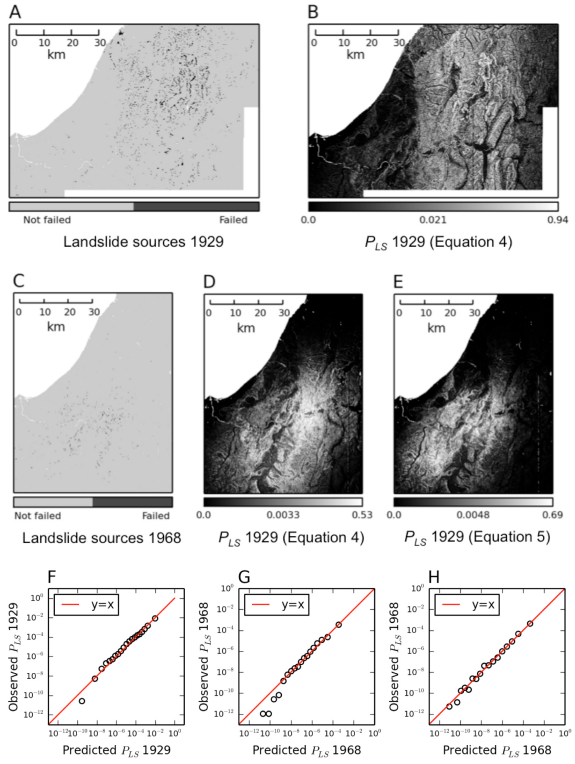

Figure 11. Comparison of observed and predicted distributions of hillslope failure. **(a)** 1929 earthquake: left – input map of hillslope failures, right – output map of predicted P_{LS} from Eq. (4). **(b)** 1968 earthquake: left – input map of hillslope failures, middle – output map of predicted P_{LS} from Eq. (4) (Fault distance model), right – output map of predicted P_{LS} from Eq. (5) (PGA model). **(c)** Plots of observed vs. predicted P_{LS}. Note that these data are generated by aggregating probabilities across 20 equal quantile bins of the predicted P_{LS}.

ESURFD
3, 1–52, 2015

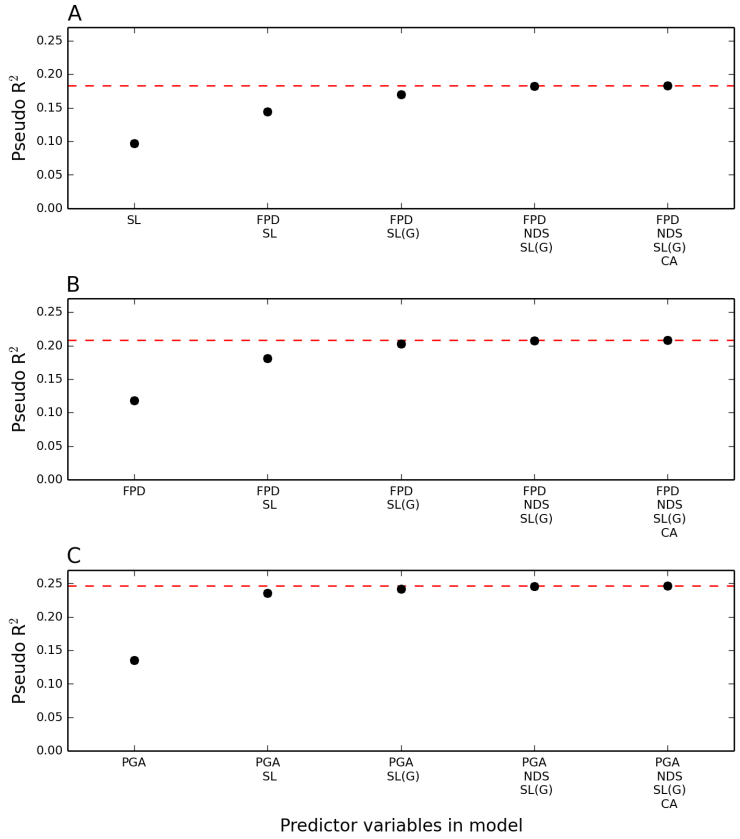

Figure 12. Plots showing the relative contribution of predictor variables to the fit of the 1929 and 1968 hillslope failure probability models. Sequence of model input predictors and resulting pseudo-R^2 goodness of fit values, produced by sequentially removing the least contributing predictor variable. **(a)** Equation (4) breakdown for the 1929 earthquake, **(b)** Eq. (4) breakdown for the 1968 earthquake, **(c)** Eq. (5) breakdown for the 1968 earthquake.

ESURFD
3, 1–52, 2015

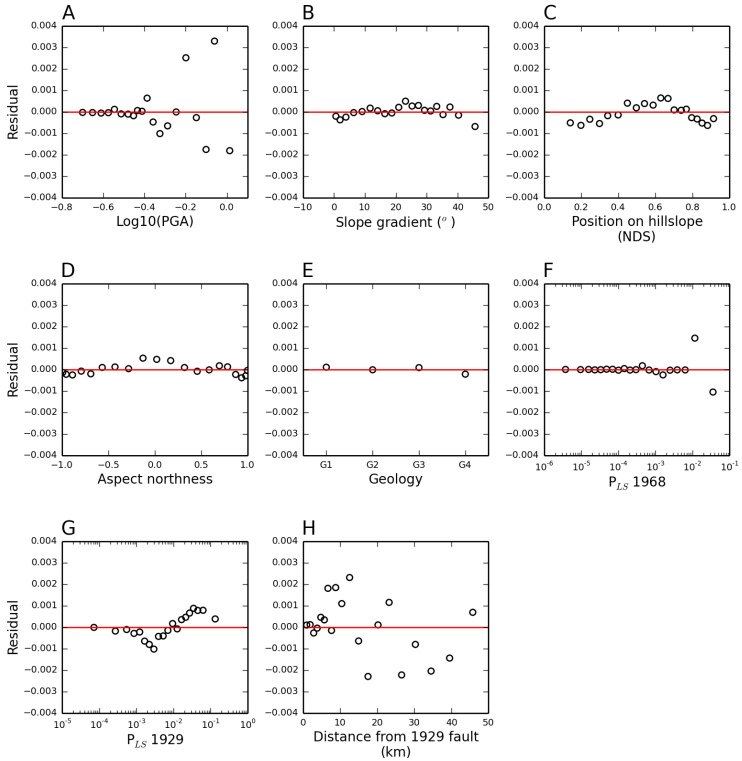

Figure 13. Distributions of P_{LS} residuals for the 1968 earthquake, hindcast using Eq. (5). **(a–e)** show the residuals for this model (observed P_{LS} minus predicted P_{LS}) plotted against each of the model predictors. **(f)** shows the model residuals plotted against the predicted P_{LS}. **(g)** and **(h)** show the model residuals plotted against predicted P_{LS} for the 1929 earthquake and distance from the 1929 coseismic fault, respectively. All residuals are calculated by aggregating probabilities across 20 equal quantile bins of the x variable. Note that positive residuals indicate that the model under-predicts P_{LS} and negative residuals indicate that the model over-predicts P_{LS}.

ESURFD
3, 1–52, 2015

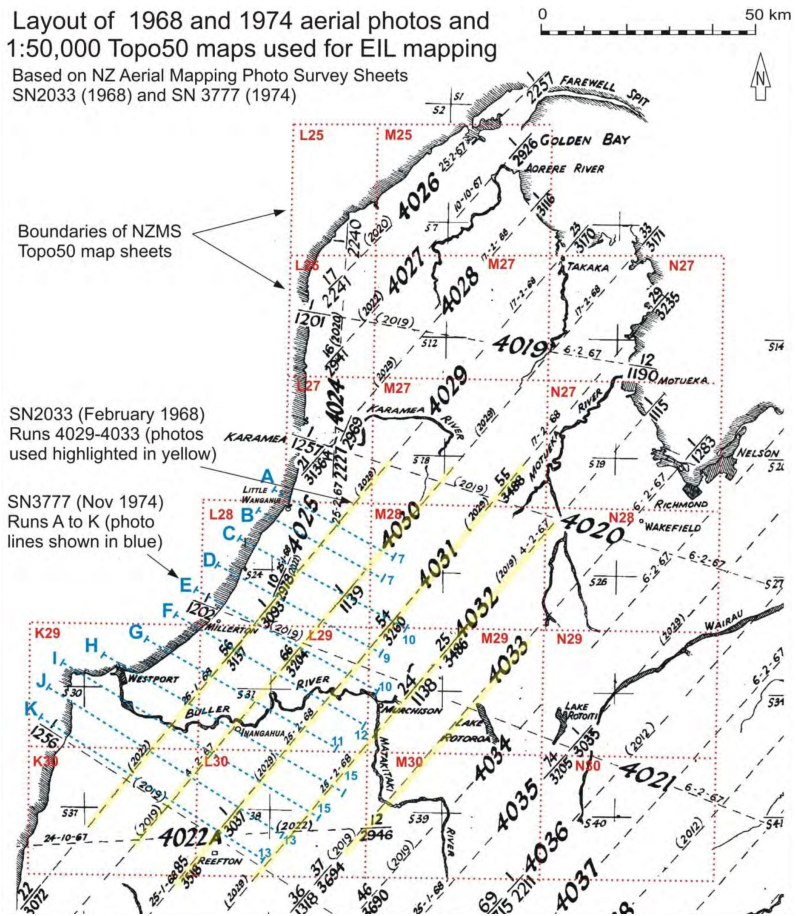

Figure A1. Map showing the layout and location of aerial photo surveys SN2033 and SN3777, aerial photo runs and areas of 1 : 50 000 topographic maps used in the mapping of landslides caused by the 1929 and 1968 earthquake.

ESURFD
3, 1–52, 2015

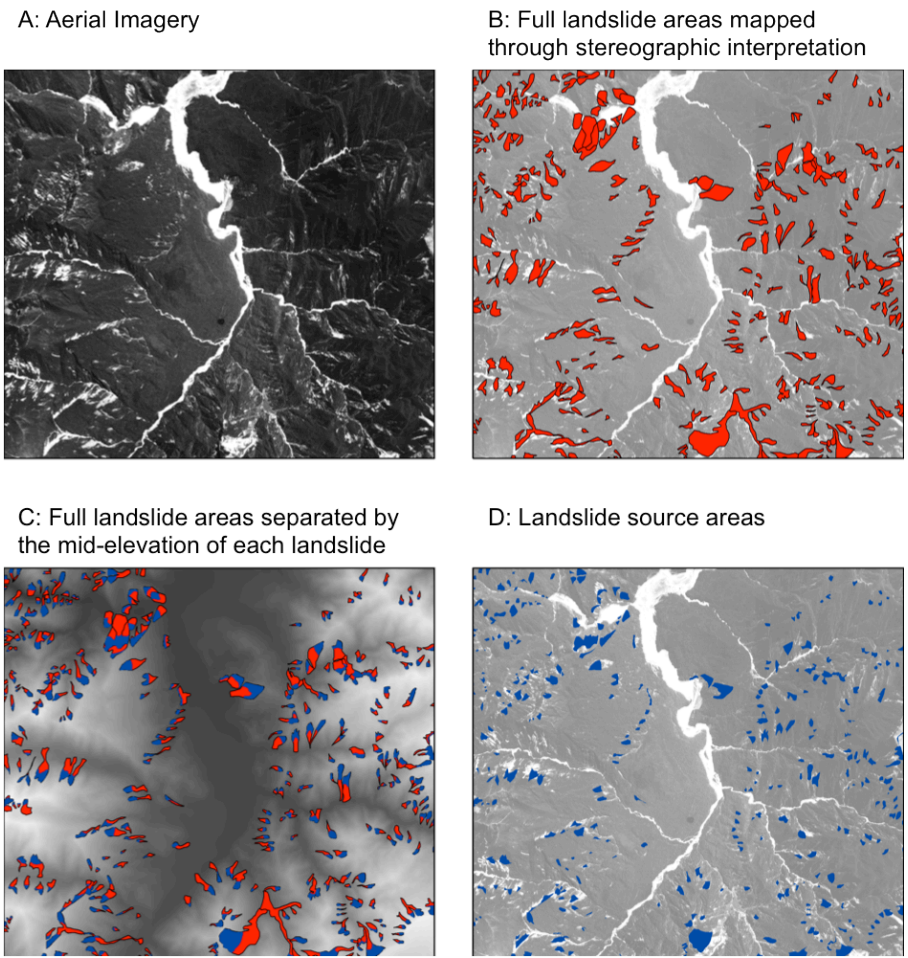

Figure B1. Illustration of landslide source area extraction technique for a 10 km × 10 km sample area, showing landslides triggered by the 1929 Buller earthquake.

ESURFD
3, 1–52, 2015

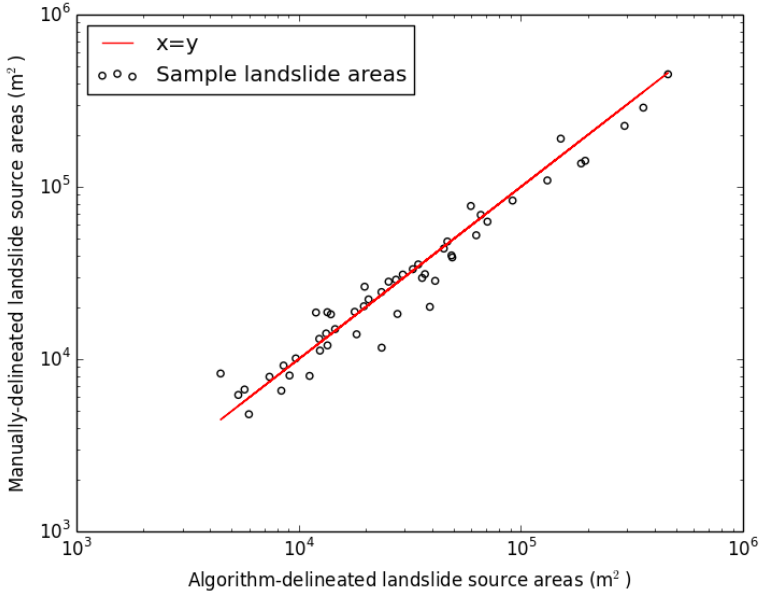

Figure B2. Comparison of visually- and algorithm-delineated source areas, for a sample of 51 landslides. Manually and automatically delineated areas fit closely to a 1 : 1 line, showing that this technique can provide an accurate approximation of the landslide source area.

ESURFD
3, 1–52, 2015